Bull Earthquake Eng (2006) 4:295–318
DOI 10.1007/s10518-006-9015-0

ORIGINAL RESEARCH PAPER

Seismic displacement of gravity walls by a two-body model

Constantine A. Stamatopoulos · Eleni G. Velgaki · Arezou Modaressi · Fernando Lopez-Caballero

Received: 7 February 2004 / Accepted: 10 February 2006 /
Published online: 1 July 2006

Abstract Gravity walls retaining dry soil are modeled as a system of two bodies: (a) the gravity wall that slides along the wall-foundation soil boundary and (b) the critical soil wedge in the soil behind the wall. The strength of the system is defined by both the frictional and the cohesional components of resistance. The angle of the prism of the critical soil wedge behind the wall is obtained using the limit equilibrium method. The model accounts for changes in the geometry of the backfill soil behind the wall by considering the displacements at the end of each time step under limit equilibrium. The model shows that the standard (single) block model is over-conservative for the extreme case of critical-to-applied-seismic acceleration ratios less than about 0.30, but works well for cases where this ratio ranges between 0.5 and 0.8. The model is applied to predict the seismic displacement of gravity walls (a) tested in the shaking-table and (b) studied numerically by elaborate elasto–plastic analyses.

Keywords Gravity walls · Critical acceleration · Seismic displacement · Large displacement · Critical rupture angle · Sliding-block models

Abbreviations

B	backfill (=retained soil)
B-cr	the critical soil wedge at the backfill next to the wall
FEM	Finite element method
i	increment

Communicated by C. A. Stamatopoulos

C. A. Stamatopoulos (✉)· E. G. Velgaki
Stamatopoulos and Associates Co. Ltd.,
5 Isavron st., Athens 114–71, Greece
e-mail: k.stam@saa-geotech.gr

A. Modaressi · F. Lopez-Caballero
Laboratoire de mecanique des sols, structures, materiaux, Ecole Centrale Paris,
Paris, France

I	interface
MO	Mononobe-Okabe method
0	initial configuration
RE	the Richards–Elms method
s	seconds
sl	sliding-block model
W	wall

Notations

a_{m}	The maximum value of the acceleration in the applied acceleration history
$b_{\mathrm{Bcr-i}}$	The contact length of the critical soil wedge with the retained soil at increment "*i*"
$b_{\mathrm{B-i}}$	The contact length of a soil wedge with inclination not necessarily equal to the critical with the retained soil at increment "*i*"
b_{W}	The length of the base of the wall
$c_{\mathrm{B}}, c_{\mathrm{w}}, c_{\mathrm{I}}$	The cohesional component of resistance (a) in the retained soil, (b) at the wall- foundation soil interface and (c) at the wall-backfill interface, respectively.
d	differential
d_i	The length of the soil-retaining wall interface at increment "*i*"
g	the acceleration of gravity
H_0	The height of the soil behind the wall at the initial configuration (Fig. 1)
H_i	The height of the soil behind the wall at increment "*i*"
$k_{\mathrm{c-0}}$	The critical horizontal acceleration factor for relative motion of the wall-retaining soil system of Fig. 1 (at the initial configuration)
$k_{\mathrm{c-}i}$	The critical horizontal acceleration factor for relative motion of the wall-retaining soil system of Fig. 1 at increment "*i*"
$k_{\mathrm{c-B-}i}$	The horizontal acceleration factor for relative motion of the wall-backfill system at increment "*i*" when the soil wedge behind the wall that slides has inclination $\alpha_{\mathrm{B-}i}$
$k_{\mathrm{c-RE}}$	The critical horizontal acceleration factor for relative motion of the wall-backfill system, according the Richards-Elms method (=$\mathrm{k_{c-0}}$)
$k_{\mathrm{c-sl}}$	The critical horizontal acceleration factor for relative motion of the sliding-block model
$k(t)g$	The applied horizontal acceleration history
k_ig	The applied horizontal acceleration at increment "*i*"
$P_{\mathrm{a-MO}}$	The lateral force estimated by the MO method
$S_{\mathrm{W-i}}, S_{\mathrm{B-i}}, S_{\mathrm{I-i}}$	Dimensionless parameters given by Eq. 7b
$S_{\mathrm{W-0}}, S_{\mathrm{B-0}}, S_{\mathrm{l-0}}$	Dimensionless parameters given by Eq. 7b by replacing the subscript "*i*" with the subscript "0"
X_{i}	Dimensionless parameter given by Eq. 7a

X_0	Dimensionless parameter given by Eq. 7a by replacing the subscript "i" with the subscript "0"
t	time
u_{W}	The absolute value of the distance moved by the wall
$u_{\mathrm{W-nogech}}$	The wall displacement when changes in geometry are neglected
u_{sl}	The absolute value of the distance moved by the sliding-block model
V_{s}	Shear wave velocity
$W_{\mathrm{Bcr}-i}$	The weight of the critical soil wedge at increment "i"
$W_{\mathrm{B}-i}$	The weight of the soil wedge with inclination not necessarily equal to the critical at increment "i"
W_{w}	The weight of the wall
$Z_{\mathrm{W}-i}$	The factor defined by Eq. 3b
$Z_{\mathrm{W}-0}$	The factor defined by Eq. 3b by replacing the subscript "i" with the subscript "0"
$Z_{\mathrm{Bcr}-0}$	The factor defined by Eq. 12b

Greek

α_{W}	The inclination of the base of the wall
$\alpha_{\mathrm{Bcr}-i}$	The inclination of the base of the critical soil wedge at increment "i"
$\alpha_{\mathrm{B}-i}$	The inclination of the base of the soil wedge not necessarily equal to the critical at increment "i"
$\alpha_{\mathrm{Bcr}-0}$	The inclination of the base of the critical soil wedge at the initial configuration
γ	The unit weight of the soil behind the wall
δ	Angle defining the inclination of the wall-retained soil interface (Fig. 1)
$\Delta\vec{u}_{\mathrm{W}-i}$	the distance moved by the wall at increment "i"
$\Delta\vec{u}_{\mathrm{B-cr}-i}$	The incremental distance moved by the backfill at increment "i"
θ	The inclination of the soil behind the wall (Fig. 1)
λ_i	The factor defined by Eq. 1
$\phi_{\mathrm{B}}, \phi_{\mathrm{w}}, \phi_{\mathrm{I}}$	The frictional component of resistance (a) in the retained soil, (b) at the wall- foundation soil interface and (c) at the wall-backfill interface, respectively

Introduction

The concept of allowable displacements, as the basis of seismic design of gravity walls, has been gaining in importance (e.g. Whitman 1990; Iai 2001). Simplified models predicting seismic ground displacements are less accurate than methods using finite-elements and elasto–plastic constitutive models, but have the advantage of simplicity that makes them accessible to practicing engineers. In addition, they are effective in performing parametric analyses, which are often needed in geotechnical engineering, as the value of soil parameters and the input earthquake motion are usually not known with confidence.

Simplified analyses predicting the seismic displacement of gravity walls under a horizontal seismic excitation are based on the Mononobe–Okabe (MO) method and Newmark's sliding-block model (e.g. Iai 2001). The MO method (Mononobe 1924; Okabe 1924) estimates the lateral force, P_{a-MO}, on gravity walls retaining dry soil by using frictional resistance and inertia forces. The force P_{a-MO} acts on the wall from the wedge in the soil behind the wall with inclination that corresponds to the maximum pressure applied on the wall.

Newmark's model (Newmark 1965) consists of a block on an inclined plane. Critical acceleration factor, k_{c-sl}, is the minimum factor that when multiplied by the acceleration of gravity, g, gives the horizontal acceleration which is just sufficient to cause movement of the block. Every time during the earthquake that the applied horizontal acceleration is larger than the critical acceleration ($k_{c-sl}\, g$), the block slides downwards. The total displacement of the block is equal to the sum of these partial displacements that are caused by the momentary slides.

The above-mentioned method for the prediction of seismic displacement of gravity walls has been initially proposed by Richards and Elms (RE) (1979). In the RE approach, the force acting on the wall by the retained soil is estimated by the MO method, as a function of the seismic acceleration applied on the retained soil. The critical horizontal acceleration factor for relative motion of the wall-backfill system, denoted as $\{k_{c-RE}\}$, is estimated by considering the equilibrium of forces acting on the wall. As in the condition of limiting equilibrium the seismic acceleration acting on the retained soil equals (by definition) the critical acceleration, k_{c-RE} must be obtained by iteration (Iai 2001). For best predictions (e.g. Kotta et al. 1988), the applied acceleration history is estimated by equivalent linear dynamic analyses that consider the dynamic characteristics of the backfill. The seismic displacement of the wall is estimated using the critical acceleration factor k_{c-RE}, and the applied acceleration history. In particular, it is assumed that the seismic displacement of the wall is equal to the seismic displacement of Newmark's sliding block with similar critical acceleration when the same applied seismic excitation is applied.

Recently, Stamatopoulos and Velgaki (2001a) proposed a model of a two-body system of kinematically compatible components to predict the seismic displacement of gravity walls. Even though extensions of the RE model had been developed (e.g. Zarrabi-Kashani 1979), such a kinematically compatible model predicting the seismic displacement of gravity walls had not been proposed previously. Consistently with the RE method mentioned above, the configuration of the wall-backfill system was modeled using two bodies: (a) the wall that slides along the wall-foundation soil and (b) the wedge that slides along the plane of least resistance in the retained soil. Analytical expressions giving (1) the angle of the prism of the soil wedge, and (2) the corresponding value of the critical acceleration were obtained using the principle of limit equilibrium.

As described by Stamatopoulos and Velgaki (2001a), the new method generally produces an interface force between the wall and the retained soil, which is different from the MO force. Yet, just prior to relative movement, the two methods predict similar interface forces. The reason is that the MO solution was obtained using the equilibrium of only the critical wedge in the retained soil, while the new solution considers the equilibrium of a two-body system that includes both the wall and the critical soil wedge. Only just prior to relative movement, the dynamic effects of the wall do not affect the solution. As a consequence, the new method predicts similar critical acceleration, but different seismic wall displacement than the RE approach.

Stamatopoulos and Velgaki (2001a, b) considered the simplified case of (a) only frictional soil resistance and (b) small wall displacement, where the effect of the deformation of the retained soil on forces can be neglected. The present study extends the simplified case to the general one of (a) both frictional and cohesional components of resistance and (b) both small and large wall displacements.

Model outline

Figure 1 gives the geometry of the wall-backfill system considered. The problem is defined by (a) characteristics of the wall: its weight per unit length W_w, the inclination of its base, α_W, the inclination of its interface with the retained soil $(90° - \delta)$, and the width of its foundation, b_W, (b) characteristics of the soil behind the wall: its inclination to the horizontal, θ, its unit weight, γ, and its height at the wall interface, H_0, (c) the frictional and cohesional components of strength (1) in the retained soil, ϕ_B and c_B, (2) at the wall - foundation soil interface ϕ_w and c_w, and (3) at the wall-backfill interface ϕ_I and c_I and (d) the horizontal applied seismic acceleration history $\{k(t)g\}$, where $k(t)$ is a dimensionless function of time, and g is the acceleration of gravity. The geometry is assumed dry (i.e. above the water table).

The seismic movement of the wall-backfill system of Fig. 1 is modeled using the two-body sliding system of Fig. 2. Total contact is assumed between the two bodies. At the initial configuration, the first body corresponds to the gravity wall and the second to the critical wedge in the soil behind the wall. According to the limiting equilibrium method (e.g. Sarma 1999), the inclination of this wedge in the soil behind the wall is the inclination that produces instability with the minimum possible applied horizontal acceleration.

As a result of the applied shaking, gravity walls move outwards, away from the retained soil. Assuming that contact always exists between the wall and the retained soil, the outward wall movement causes deformation of the retained soil near the wall. In typical walls, the resistance on the wall-backfill interface is less than on any other internal sub-planes in the retained soil. It is inferred that, according to the law of limit equilibrium (where the slip surface develops at the location where relative motion occurs for the least value of applied acceleration), the internal slip sub-plane between the two bodies should remain in the wall-backfill interface. This implies that the first

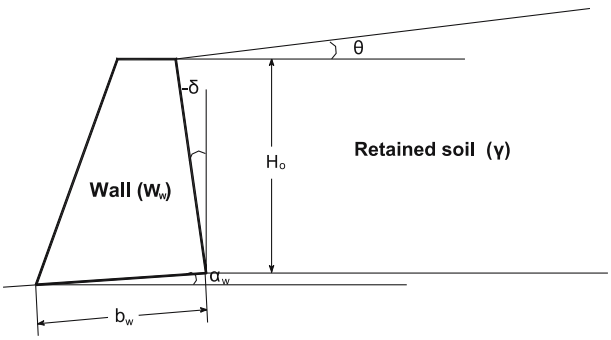

Fig. 1 Gravity wall and retained soil geometry considered in the present study

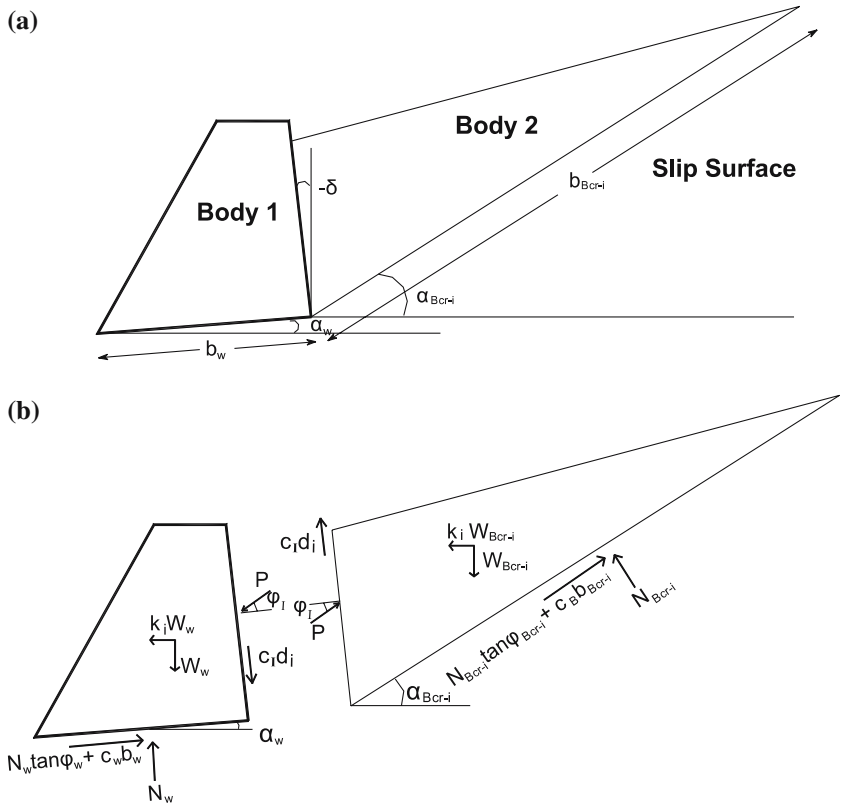

Fig. 2 The two-body sliding system used to predict the seismic displacement of the wall-backfill system of Fig. 1: **a** Geometry and **b** forces acting in the two bodies

body of the two-body system is always the wall, while the second body is always part of the soil behind the wall.

Unlike the first body, the second body changes its shape with displacement. The analysis is performed incrementally with seismic excitation $k(t)$ applied in small time increments. The change in shape of the second body can be determined by applying the limit equilibrium condition at each time step.

Analytical solution algorithm

Wall–soil interaction

At each time increment "i", the seismic excitation is k_i and the parameters that define (a) the inclination of the base, the weight, the contact length of (i) the first body and (ii) the second body of Fig. 2 and (b) the interface angle and length between the two bodies, are (a) (i) $\alpha_{\rm w}, W_{\rm w}, b_{\rm w}$, (ii) $\alpha_{{\rm Bcr}-i}, W_{{\rm Bcr}-i}, b_{{\rm Bcr}-i}$ and (b) δ and d_i, respectively. The parameters $\alpha_{{\rm Bcr}-i}, W_{{\rm Bcr}-i}, b_{{\rm Bcr}-i}$ and d_i are not known a priori, and depend on the distance moved. The algorithm estimating them is given later. In addition, the strengths below both bodies and at the interface are (a) $\phi_{\rm w}$ and $c_{\rm w}$, (b) $\phi_{\rm B}$ and $c_{\rm B}$ and (c) $\phi_{\rm I}$ and $c_{\rm I}$, respectively.

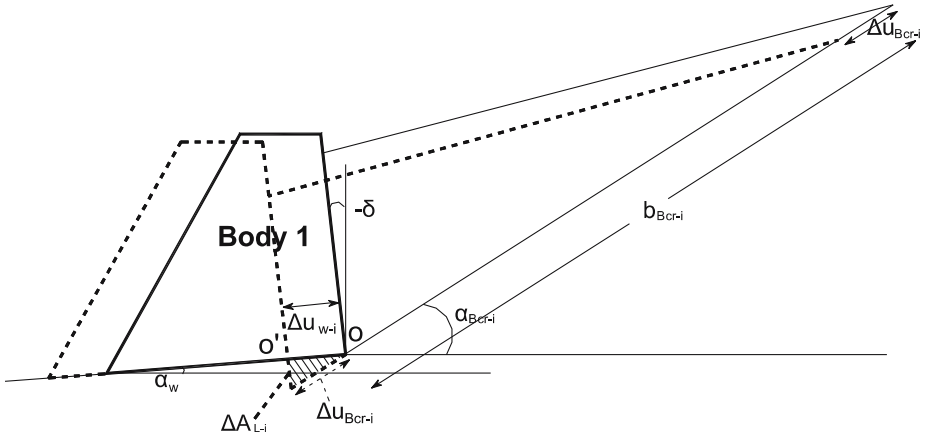

Fig. 3 The deformation of the wall-backfill system with displacement at increment "*i*". The *solid* and *dotted lines* give the initial and final configurations of the increment, respectively. The increment $\Delta u_{\mathrm{W}-i}$ is shown *large* for clarity. *Points O and O′* are the points where the slip sub-planes in the backfill start of increments "*i*" and "$i+1$", respectively

At each increment, the first body (or the wall) is displaced by $\Delta\vec{u}_{\mathrm{W}-i}$ along the wall–foundation soil interface (Fig. 3). The second body (or the critical wedge behind the wall) is displaced by $\Delta\vec{u}_{\mathrm{Bcr}-i}$ along the slip surface of the backfill. Unlike $\Delta\vec{u}_{\mathrm{Bcr}-i}$, the direction of $\Delta\vec{u}_{\mathrm{W}-i}$ does not change in the analysis. Thus, the absolute value of the distance moved by the wall, u_{w}, equals the sum of all the absolute values of $\Delta\vec{u}_{\mathrm{W}-i}$s.

It is assumed that at each time increment the total contact between the two bodies of Fig. 2 is retained along the shearing surface. Thus, the component of the movement perpendicularly to this surface should be the same for both moving bodies, or,

$$\frac{\Delta u_{\mathrm{W}-i}}{\Delta u_{\mathrm{Bcr}-i}} = \frac{\cos(-\delta-\alpha_{\mathrm{Bcr}-i})}{\cos(-\delta-\alpha_{\mathrm{W}})} = \lambda_i, \tag{1}$$

where at increment "*i*", $\Delta u_{\mathrm{W}-i}$ and $\Delta u_{\mathrm{Bcr}-i}$ are the absolute value of displacements in the direction of movement of the wall and backfill wedge respectively.

Figure 2b gives the forces acting in the two bodies. The equation of motion of the first body, in the direction of sliding is:

$$\begin{aligned}\frac{W_{\mathrm{W}}}{g}(\mathrm{d}^2u_{\mathrm{W}}/\mathrm{d}t^2) = \frac{1}{\cos\,\phi_{\mathrm{W}}}\cdot[&W_{\mathrm{W}}\sin(\alpha_{\mathrm{W}}-\phi_{\mathrm{W}}) + P_{\mathrm{a}}\cos(\phi_{\mathrm{I}}+\phi_{\mathrm{W}}-\alpha_{\mathrm{W}}-\delta)\\ &-c_{\mathrm{W}}b_{\mathrm{W}}\cos\,\phi_{\mathrm{W}} - c_{\mathrm{I}}d_i\sin(\phi_{\mathrm{W}}-\delta-\alpha_{\mathrm{W}}) + k_iW_{\mathrm{W}}\cos(\alpha_{\mathrm{W}}-\phi_{\mathrm{W}})\big].\end{aligned} \tag{2a}$$

Similarly, at each increment, the equation of motion of the second body in the sliding direction is:

$$\begin{aligned}\frac{W_{\mathrm{Bcr}-i}}{g}(\mathrm{d}^2u_{\mathrm{Bcr}-i}/\mathrm{d}t^2) = \frac{1}{\cos\,\phi_{\mathrm{B}}}\cdot\big[&W_{\mathrm{Bcr}-i}\sin(\alpha_{\mathrm{Bcr}-i}-\phi_{\mathrm{B}})\\ &-P_{\mathrm{a}}\cos(\phi_{\mathrm{I}}+\phi_{\mathrm{B}}-\alpha_{\mathrm{Bcr}}-\delta) - c_{\mathrm{B}}b_{\mathrm{Bcr}-i}\cos\phi_{\mathrm{B}}\\ &+c_{\mathrm{I}}d_i\sin(\phi_{\mathrm{B}}-\delta-\alpha_{\mathrm{Bcr}-i}) + k_iW_{\mathrm{Bcr}-i}\cos(\alpha_{\mathrm{Bcr}-i}-\phi_{\mathrm{B}})\big].\end{aligned} \tag{2b}$$

The governing equation of the sliding system is obtained from Eqs. (1), (2a) and (2b) as

$$\mathrm{d}^2 u_{\mathrm{W}}/\mathrm{d}t^2 = Z_{\mathrm{W}-i} g(k_i - k_{\mathrm{c}-i}), \tag{3a}$$

where

$$Z_{\mathrm{W}-i} = \frac{W_{\mathrm{W}} \cos(\alpha_{\mathrm{W}} - \phi_{\mathrm{W}}) \cos(\phi_{\mathrm{I}} - \alpha_{\mathrm{Bcr}-i} - \delta + \phi_{\mathrm{B}}) + W_{\mathrm{Bcr}-i} \cos(\alpha_{\mathrm{Bcr}-i} - \phi_{\mathrm{B}}) \cos(\phi_{\mathrm{I}} - \alpha_{\mathrm{W}} - \delta + \phi_{\mathrm{W}})}{W_{\mathrm{W}} \cos\phi_{\mathrm{W}} \cos(\phi_{\mathrm{I}} - \alpha_{\mathrm{Bcr}-i} - \delta + \phi_{\mathrm{B}}) \lambda_{\mathrm{i}} + W_{\mathrm{Bcr}-i} \cos\phi_{\mathrm{B}} \cos(\phi_{\mathrm{I}} - \alpha_{\mathrm{W}} - \delta + \phi_{\mathrm{W}})} \lambda_i \tag{3b}$$

and

$$k_{\mathrm{c}-i} = \mathrm{AA}/\mathrm{BB}, \tag{3c}$$

where

$$\begin{aligned}
\mathrm{AA} = {} & \left[W_{\mathrm{W}} \sin(\phi_{\mathrm{W}} - \alpha_{\mathrm{W}}) + c_{\mathrm{W}} b_{\mathrm{W}} \cos\phi_{\mathrm{W}}\right] \cos(\phi_{\mathrm{I}} + \phi_{\mathrm{B}} - \alpha_{\mathrm{Bcr}\text{-}i} - \delta) \\
& + \left[W_{\mathrm{Bcr}\text{-}i} \sin(\phi_{\mathrm{B}} - \alpha_{\mathrm{Bcr}\text{-}i}) + c_{\mathrm{B}} b_{\mathrm{Bcr}\text{-}i} \cos\phi_{\mathrm{B}}\right] \cos(\phi_{\mathrm{I}} + \phi_{\mathrm{W}} - \alpha_{\mathrm{W}} - \delta) \\
& + c_{\mathrm{I}} d_{\mathrm{i}} \cos\phi_{\mathrm{I}} \cos(\phi_{\mathrm{W}} - \phi_{\mathrm{B}} + \alpha_{\mathrm{W}} - \alpha_{\mathrm{Bcr}\text{-}i}), \\
\mathrm{BB} = {} & W_{\mathrm{W}} \cos(\phi_{\mathrm{W}} - \alpha_{\mathrm{W}}) \cos(\phi_{\mathrm{I}} + \phi_{\mathrm{B}} - \alpha_{\mathrm{Bcr}\text{-}i} - \delta) \\
& + W_{\mathrm{Bcr}\text{-}i} \cos(\phi_{\mathrm{B}} - \alpha_{\mathrm{Bcr}\text{-}i}) \cos(\phi_{\mathrm{I}} + \phi_{\mathrm{W}} - \alpha_{\mathrm{W}} - \delta).
\end{aligned}$$

Definition of the critical soil wedge

As will be illustrated later, the only shape factor in the parameters of Fig. 1 defining the geometry of the backfill that changes as the wall is displaced is the backfill height. At increment "i", this height is denoted as H_i.

The interface length of the two bodies can be expressed in terms of H_i and δ as

$$d_i = H_i/\cos(-\delta). \tag{4}$$

Also, at increment "i" the length of a potential slip surface and the weight of a soil wedge behind the wall with inclination not necessarily equal to the critical, denoted as $b_{\mathrm{B}-i}$ and $W_{\mathrm{B}-i}$, respectively, can be expressed in terms of the corresponding inclination of the soil wedge behind the wall, $\alpha_{\mathrm{B}-i}$, as:

$$b_{\mathrm{B}-i} = H_i \frac{1 - \tan\delta \tan\theta}{\cos\alpha_{\mathrm{B}-i}(\tan\alpha_{\mathrm{B}-i} - \tan\theta)}, \tag{5}$$

$$W_{\mathrm{B}-i} = 0.5\gamma H_i^2 \frac{(1 - \tan\alpha_{\mathrm{B}-i} \tan\delta)(1 - \tan\delta\tan\theta)}{\tan\alpha_{\mathrm{B}-i} - \tan\theta}. \tag{6}$$

In addition, the following dimensionless symbols are introduced:

$$X_i = 2W_{\mathrm{W}}/(\gamma H_i^2), \tag{7a}$$

$$S_{\mathrm{W}-i} = 2c_{\mathrm{W}} b_{\mathrm{W}}/(\gamma H_i^2), \quad S_{\mathrm{B}-i} = 2c_{\mathrm{B}}/(\gamma H_i), \quad S_{\mathrm{I}-i} = 2c_{\mathrm{I}}/(\gamma H_i). \tag{7b}$$

Then, according to Eq. 3c, the horizontal acceleration factor for relative motion of the two-body system of Fig. 2 when the angle of inclination of the soil wedge is $\alpha_{\mathrm{B}-i}$ equals

$$k_{\mathrm{cB}-i} = \mathrm{AA_B}/\mathrm{BB_B}, \tag{8a}$$

where:

$$\begin{aligned} AA_B = & \left\{X(G-M)+S_{W-i}\sqrt{1+M^2}+S_{I-i}\left[G-M-(1+GM)D\right]\right\} \\ & \cdot\left[(1+AB)(1+FD)-(B-A)(F-D)\right] \\ & +\left\{(DA_i-1)\frac{DK-1}{A_i-K}\cdot(B-A_i)+S_{B-i}\cdot\left(1+A_i^2\right)\cdot\frac{1-DK}{A_i-K}\right. \\ & \left.-S_{I-i}\left[B-A_i-(1+A_iB)D\right]\right\}\cdot\left[(1+GM)(1+FD)-(G-M)(F-D)\right] \end{aligned} \tag{8b}$$

and

$$\begin{aligned} BB_B = & X\cdot(1+MG)\cdot\left[(1+FD)(1+A_iB)-(F-D)(B-A_i)\right] \\ & +\frac{(DK-1)(DA_i-1)}{A_i-K}\cdot(1+A_iB)\cdot\left[(1+FD)(1+GM)-(F-D)(G-M)\right], \end{aligned} \tag{8c}$$

where

$M=\tan\alpha_W, D=\tan\delta, K=\tan\theta, B=\tan\phi_B, G=\tan\phi_W, F=\tan\phi_I, A_i=\tan\alpha_{B-i}$.

The critical rupture angle α_{Bcr-i} corresponds to the value of α_{B-i} that minimizes k_{cB-i} in Eq. 8. An analytical solution estimating α_{Bcr-i} is given by Stamatopoulos et al. (2001). Alternatively, α_{Bcr-i} can be obtained numerically by searching the factor α_{B-i} that minimizes k_{cB-i} in Eq. 8. As illustrated by Stamatopoulos et al. (2001), k_{cB-i} is a parabola in terms of $(\tan\alpha_{B-i})$, having a single well-defined minimum. It is inferred that estimating numerically $(\tan\alpha_{Bcr-i})$, and thus α_{Bcr-i} also, is a simple matter using for example the bisection method (e.g. Dahlquist and Bjorck 1974).

Once the inclination α_{Bcr-i} has been obtained, W_{Bcr-i} and b_{Bcr-i} can also be obtained from $H_i, \delta, \theta, \alpha_{Bcr-i}$ and γ, using Eqs. 5 and 6 by replacing α_{B-i} with α_{Bcr-i}.

Changes of geometry with outward wall displacement

It was stated above that the wall at each time increment "i" is displaced outwards by $\Delta\vec{u}_{W-i}$, while the critical soil wedge is displaced by $\Delta\vec{u}_{Bcr-i}$. Figure 3 gives, in enlarged scale of incremental displacement, the induced deformation. It can be observed that the only shape factor in the parameters of Fig. 1 defining the backfill that changes as the wall is displaced is the backfill height. In particular, the height of the backfill at increment "i" equals

$$H_i = H_0 - \sum_{k=1}^{i-1}\left[\Delta u_{w-k}((\sin\alpha_{Bcr-k})/\lambda_k - \sin\alpha_w)\right]. \tag{9}$$

Figure 3 also shows that a part of the cross-sectional area of the backfill, denoted as ΔA_{L-i}, is lost in the analysis. Yet, when the increment Δu_{W-i} is sufficiently small, the effect of the lost part can be neglected. The reason is that this area is proportional to the square of (the small increment) Δu_{W-i}.

Once the deformed shape is estimated, the new inclination of the critical soil wedge from the new point at the base of the wall-backfill interface (point O′ of Fig. 3), must be estimated with the procedure described in Sect. 'Definition of the critical soil wedge'.

Computer program

A computer program was written by the first two authors, that predicts the seismic displacement of gravity walls retaining dry soil, according to the model given above. The input required by the computer program includes (a) the nodes defining the wall geometry, (b) the parameters $W_w, \theta, \gamma, H_0, \phi_B, c_B, \phi_w, c_w, \phi_I$ and c_I and (c) the applied horizontal excitation. Numerical integration is performed after every time increment "i" of the acceleration history record using the Euler's method (e.g. Dahlquist and Bjorck 1974). At each increment, H_i is updated and iteration is performed to estimate the new inclination of the slip surface, α_{Bcr-i}. Graphics illustrating the final geometry of the wall-retaining soil system are included in the computer program. Parametric analyses using different time steps illustrated that a time step of 0.01 s, typically used in acceleration history records found in the literature, produces adequate accuracy of both the numerical integration and the simulation of retained soil deformation, at least for wall displacement less than 2 m.

In addition to the analyses described above, the computer program can perform analyses without considering the effects of changes in the geometry of the backfill. In this case, iteration is used to estimate the inclination of the slip surface at the initial configuration, α_{Bcr-0}, and during the analysis the changes in weight, inclination and contact length of the critical soil wedge behind the wall are not updated with the distance moved.

The computer program was used in the analyses given below.

Parametric analyses

Initial configuration

The most important parameter in sliding-block analyses is the critical acceleration at the initial configuration, k_{c-0}, as for any given seismic acceleration history it greatly affects the magnitude of seismic displacement (e.g. Ambraseys and Menu 1988). The angle α_{Bcr-0} is also a critical parameter of the present model, because, once α_{Bcr-0} is known, all parameters of the governing equation of motion (Eq. 3) at the initial wall configuration, including k_{c-0}, can be defined.

As was indicated in the introduction, sliding-block methods usually estimate the seismic displacement u_{sl} by the Newmark model. The corresponding equation that is solved (e.g. Ambraseys and Menu 1988) is usually:

$$d^2u_{sl}/dt^2 = g(k(t) - k_{c\text{-}0}) \quad \text{for} \quad du_{sl}/dt > 0. \tag{10}$$

From (1) and (3) it can be inferred that the governing equations of motion for the wall and the critical wedge of the backfill of the proposed model at the initial configuration are:

$$d^2u_W/dt^2 = Z_{W\text{-}0}\, g(k(t) - k_{c\text{-}0}), \tag{11}$$

$$d^2u_{Bcr\text{-}0}/dt^2 = Z_{Bcr\text{-}0}\, g(k(t) - k_{c\text{-}0}), \tag{12a}$$

where Z_{W-0} is the factor given by Eq. 3b when the subscript "i" is replaced by the subscript "0" and

$$Z_{Bcr-0} = Z_{W-0} \cos(-\delta - \alpha_{Bcr-0}) / \cos(-\delta - \alpha_W). \tag{12b}$$

Comparison of Eq. 10 with Eqs. (1) 11 and (2) 12 illustrates that they differ by the factors Z_{W-0} and Z_{Bcr-0}, respectively. Thus, for the case of small displacement, the factors Z_{W-0} and Z_{Bcr-0} relate the seismic displacement of the previous commonly-used method to the displacement of the wall and the retained soil, respectively of, the present model, for equal critical acceleration and applied excitation.

From the above it is inferred that parametric analyses of the factors k_{c-0}, α_{Bcr-0}, Z_{W-0} and Z_{Bcr-0} are of interest. According to the solution, these factors depend on the parameters of the problem $\alpha_W, \delta, \theta, \phi_B, \phi_W, \phi_I, X_0, S_{W\text{-}0}, S_{B-0}, S_{I-0}$. The parameters $X_0, S_{W\text{-}0}, S_{B-0}, S_{I-0}$ are given by Eqs. 7a and 7b by replacing the subscript "i" with the subscript "0".

Stamatopoulos and Velgaki (2001a, b) present parametric analyses showing the dependence of the factors $k_{c-0}, \alpha_{Bcr-0}, Z_{W-0}$ and Z_{Bcr-0} on $\phi_W, \phi_B, \phi_I, X_0, \theta$ and δ. Additional parametric analyses were performed in the present work for the case of wall-backfill systems with cohesional resistance S_{W-0}, S_{B-0} and S_{I-0} different from zero. Figures 4 and 5 give (a) k_{c-0}, (b) α_{Bcr-0}, (c) Z_{W-0} and (d) Z_{Bcr-0} as affected by changes of X_0, δ, S_{W-0} and S_{B-0}. The case of $\alpha_W = \theta = \delta = 0°$ and $\phi_W = \phi_B = 2\phi_I = 20°$ is presented in Fig. 4. The case of $\alpha_W = \theta = 0°, X = 1$ and $\phi_W = \phi_B = 2\phi_I = 20°$ is presented in Fig. 5.

The results of Figs. 4c, d, and 5c, d and the results of Stamatopoulos and Velgaki (2001a, b) illustrate that for typical walls where $X_0 > 0.5$ (1) Z_{W-0} varies between 0.65 and 1.1 and (2) Z_{Bcr-0} varies between 0.95 and 1.6. The largest value of 1.6 occurs when $X_0 = 0.5$ and $\delta = 25°$.

Effects of changes of geometry with displacement

In an effort to estimate the effect of changes in geometry in the prediction of the seismic displacement of gravity walls, the wall displacement predicted when changes in geometry are taken into account, u_W, was compared with the wall displacement when changes in geometry are neglected, denoted as $u_{W-nogech}$. In the second case, unlike the first, in the governing equation of motion (Eq. 3), the changes in weight, inclination and contact length of the critical soil wedge behind the wall are not updated with the distance moved. Different values of all the crucial factors of the model were considered. In all cases, similarly to Stamatopoulos (1996), the ratio $u_W/u_{W-nogech}$ was plotted against the ratio $\{(k_{c-0}g)/a_m\}$, where $(k_{c-0}g)$ is the critical acceleration in the initial configuration of the wall-backfill system and a_m is the maximum value of the acceleration in the applied earthquake record.

First (1) the effect of the applied seismic excitation was considered. The following accelerograms, covering a wide range of maximum acceleration, fundamental period and earthquake magnitude, were applied:

- El-Centro (CA, USA), 18/5/1940, component North–South, M (earthquake magnitude in the Richter scale)= 6.5, R (distance from the epicenter)= 5 km, a_m= 0.35 g, T_f (fundamental period)=0.6 s.
- San Fernando - (Avenue of Stars, CA, USA), 1971, component East–West, $M = 6.5, R = 40$ km, $a_m = 0.15$ g, $T_f = 0.15$ s.
- Kalamata (Greece), 13/9/1986, $M = 5.75, R = 9$ km, Municipality Building, component longitudinal component: $a_m = 0.24$ g, $T_f = 0.35$ s.
- Gazli (former USSR), 17/5/1976, $M = 7.3, a_m = 0.70$ g, $T_f = 0.1$ s.

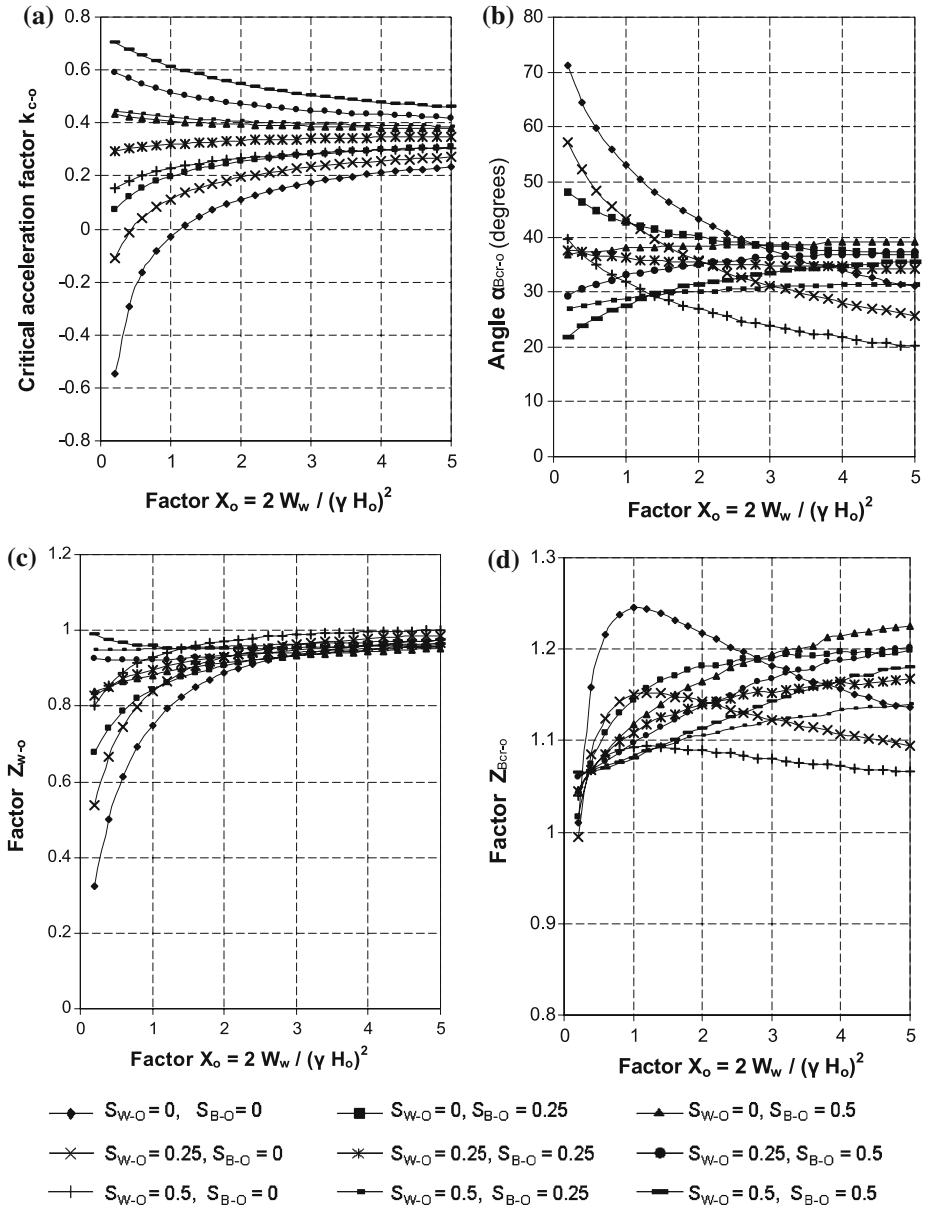

Fig. 4 The change of **a** the critical acceleration factor k_{c-0}, **b** the angle α_{Bcr-0}, **c** the factor Z_{W-0} and **d** the factor Z_{Bcr-0} in terms of X_0, S_{W-0} and S_{B-0}. The case of $\alpha_W = \theta = \delta = 0°$ and $\phi_W = \phi_B = 2\phi_I = 20°$ is presented

Then the variation of (2) the weight of the wall, (3) the inclination of the wall interface, (4) the inclination of the wall base, (5) the resistance of the wall base, (6) the length of the wall base, (7) the height of the backfill, (8) the inclination of the backfill, (9) the resistance of the backfill and (10) the resistance of the backfill-wall interface were considered. In cases (2) – (10) the El-Centro earthquake was applied. In all cases the factor k_{c-0} was varied by changing the parameter ϕ_W in increments of

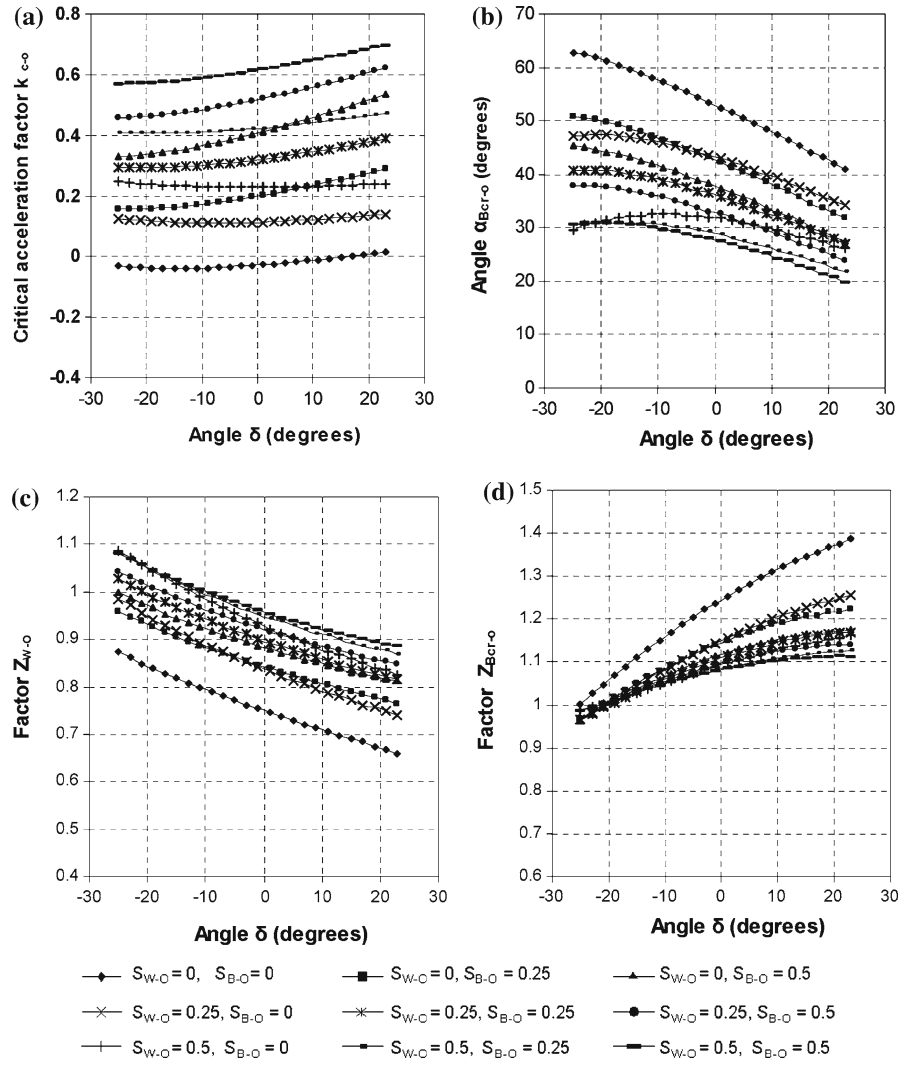

Fig. 5 The change of **a** the critical acceleration factor k_{c-0}, **b** the angle α_{Bcr-0}, **c** the factor Z_{W-0} and **d** the factor Z_{Bcr-0} in terms of δ, S_{W-0} and S_{B-0}. The case of $\alpha_W = \theta = 0°, X = 1$ and $\phi_W = \phi_B = 2\phi_I = 20°$ is presented

one degree. More specifically, the parameters used and the variations considered are described in Tables 1 and 2. The results are given in Figs. 6, 7 and 8.

As shown in Figs. 6, 7 and 8, in all cases considered, as the ratio $\{(k_{c-0}g)/a_m\}$ increases, the ratio $u_W/u_{W-nogech}$ increases towards unity. This relationship is not affected to a great extent by the values of resistances $\phi_w, c_w, \phi_B, c_B, \phi_I, c_I$, the inclinations δ, α_W, θ, the lengths H_0, b_w, the weight W_W and the applied acceleration history record. In all cases, the ratio $u_W/u_{W-nogech}$ is close to unity (greater than 0.9) when the factor $\{(k_{c-0}g)/a_m\}$ is greater than 0.3. It is inferred that the standard (single)

Table 1 List of parametric analyses performed to investigate the effect of changes in the geometry of the backfill on wall displacement. The range of ϕ_w values used and the corresponding range of $k_{c\text{-}o}$ and u_w are also given. In all cases $\gamma = 1.7\ T\text{f/m}^3$. In addition, in cases 2–10 the El Centro earthquake is applied

Case 1	Vary earthquake			
	A. El Centro	B. Kalamata	C. Gazli	D. San Fernando
$\phi_w(^\circ)$	18–34	18–28	18–44	18–25
k_{c-0}	0.0075–0.2279	0.0075–0.1425	0.0075–0.3758	0.0075–0.1011
u_w (m)	0.0066–1.6352	0.0066–0.6104	0.0071–2.6117	0.0009–0.4088
Case 2	Vary W_w			
	A. $W_w = 30$ kN/m	B. $W_w = 500$ kN/m	C. $W_w = 1000$ kN/m	D. $W_w = 1200$ kN/m
$\phi_w(^\circ)$	34–54	24–46	13–35	11–33
k_{c-0}	0.0034–0.3243	0.0112–0.3269	0.0046–0.3182	0.0043–0.3229
u_w (m)	0.0001–2.2643	0.0001–1.1911	0.0002–2.2315	0.0001–2.3722
Case 3	Vary δ			
	A. $\delta = 20^\circ$	B. $\delta = 10^\circ$	C. $\delta = -10^\circ$	D. $\delta = -20^\circ$
$\phi_w(^\circ)$	14–35	16–35	19–33	19–31
k_{c-0}	0.0097–0.2387	0.0050–0.2358	0.0077–0.2287	0.0045–0.2210
u_w (m)	0.0045–1.1959	0.0052–1.9017	0.0069–1.7190	0.0084–2.4554
Case 4	Vary α_W			
	A. $\alpha_W = 20^\circ$	B. $\alpha_W = 10^\circ$	C. $\alpha_W = -10^\circ$	D. $\alpha_W = -20^\circ$
$\phi_w(^\circ)$	1–15	8–24	28–45	38–54
k_{c-0}	0.0445–0.2395	0.0102–0.2308	0.0048–0.2395	0.0101–0.2308
u_w (m)	0.0048–0.2956	0.0060–1.3160	0.0055–2.1919	0.0074–1.5092
Case 5	Vary c_w			
	A. $c_w = 10$ kPa	B. $c_w = 20$ kPa	C. $c_w = 50$ kPa	D. $c_w = 100$ kPa
$\phi_w(^\circ)$	17–33	15–32	11–29	4–24
k_{c-0}	0.0116–0.2274	0.0030–0.2272	0.0044–0.2284	0.0055–0.2351
u_w (m)	0.0066–1.2098	0.0067–2.6936	0.0065–2.1799	0.0056–1.9306
Case 6	Vary b_w, c_W			
	A. $b_w = 2.5$ m, $c_w = 10$ kPa	B. $b_w = 10$ m, $c_w = 10$ kPa,	C. $b_w = 2.5$ m, $c_w = 50$ kPa	D. $b_w = 10$ m, $c_w = 50$ kPa
$\phi_w(^\circ)$	17–34	16–33	13–31	9–28
k_{c-0}	0.0074–0.2383	0.0041–0.2318	0.0084–0.2381	0.0073–0.2374
u_w (m)	0.0052–1.6425	0.0061–2.2606	0.0053–1.5078	0.0053–1.6515
Case 7	Vary H_0			
	A. $H_0 = 3$ m	B. $H_0 = 6$ m	C. $H_0 = 12$ m	D. $H_0 = 15$ m
$\phi_w(^\circ)$	3–16	9–25	29–45	38–52
k_{c-0}	0.0143–0.2314	0.0106–0.2474	0.0149–0.2466	0.0044–0.2330
u_w (m)	0.0066–1.2206	0.0044–1.4215	0.0043–0.9051	0.0057–1.9451
Case 8	Vary θ			
	A. $\theta = 20^\circ$	B. $\theta = 10^\circ$	C. $\theta = -10^\circ$	D. $\theta = -20^\circ$
$\phi_w(^\circ)$	25–38	20–33	16–27	15–20
k_{c-0}	0.0156–0.2330	0.0036–0.1958	0.0027–0.1376	0.0068–0.0655
u_w (m)	0.0082–2.3256	0.0101–2.3687	0.0332–2.8913	0.1788–1.8558

Table 1 continued

Case 9	Vary ϕ_B, c_B			
	A. $\phi_B = 20°$, $c_\beta = 0$	B. $\phi_B = 40°$, $c_B = 0$	C. $\phi_B = 0$, $c_B = 15\,kPa$	D. $\phi_B = 0$, $c_B = 30\,kPa$
$\phi_w(°)$	22–38	11–27	25–43	10–31
k_{c-0}	0.0137–0.2326	0.0065–0.2259	0.0119–0.1949	0.0056–0.2311
u_w (m)	0.0062–1.0558	0.0067–1.7975	0.0124–1.1682	0.0057–1.7427
Case 10	Vary ϕ_t, c_t			
	10A. $\phi_t = 10°$, $c_t = 0$	10B. $\phi_t = 20°$, $c_t = 0$	10C. $\phi_t = 10°$, $c_t = 25\,kPa$	10D. $\phi_t = 10°$, $c_t = 50\,kPa$
$\phi_w(°)$	19–35	17–32	10–27	5–22
k_{c-0}	0.0111–0.2292	0.0145–0.2275	0.0130–0.2309	0.0088–0.2307
u_w (m)	0.0063–1.2314	0.0068–1.0247	0.0065–1.1984	0.0067–1.7144

Table 2 The values of the model parameters used in the parametric analyses of Table 1

Case	Parameters										
	W_W (kN/m)	$\Delta(°)$	$\alpha_W(°)$	c_W (kPa)	b_W (m)	H_0 (m)	$\Theta(°)$	$\phi_B(°)$	c_B (kPa)	$\phi_I(°)$	c_I (kPa)
1	700	0	0	0	5	9	0	26	0	13	0
2	*	0	0	0	5	9	0	26	0	13	0
3	700	*	0	0	5	9	0	26	0	13	0
4	700	0	*	0	5	9	0	26	0	13	0
5	700	0	0	*	5	9	0	26	0	13	0
6	700	0	0	*	*	9	0	26	0	13	0
7	700	0	0	0	5	*	0	26	0	13	0
8	700	0	0	0	5	9	*	26	0	13	0
9	700	0	0	0	5	9	0	*	*	13	0
10	700	0	0	0	5	9	0	26	0	*	*

*Different values for these model parameters were used, as given in Table 1

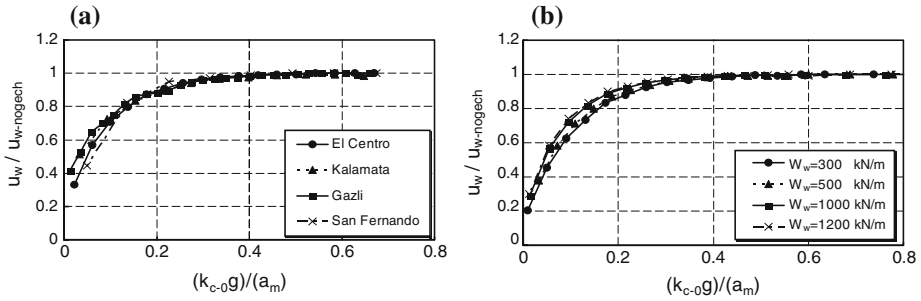

Fig. 6 The parametric analyses described in Tables 1 and 2. The ratio $u_w/u_{w-nogech}$, where $u_{w-nogech}$ is the seismic wall displacement when changes in the geometry of the soil behind the wall are neglected, versus the ratio $(k_{c-0}g)/a_m$ in terms of **a** the applied earthquake and **b** the weight of the wall, W_W

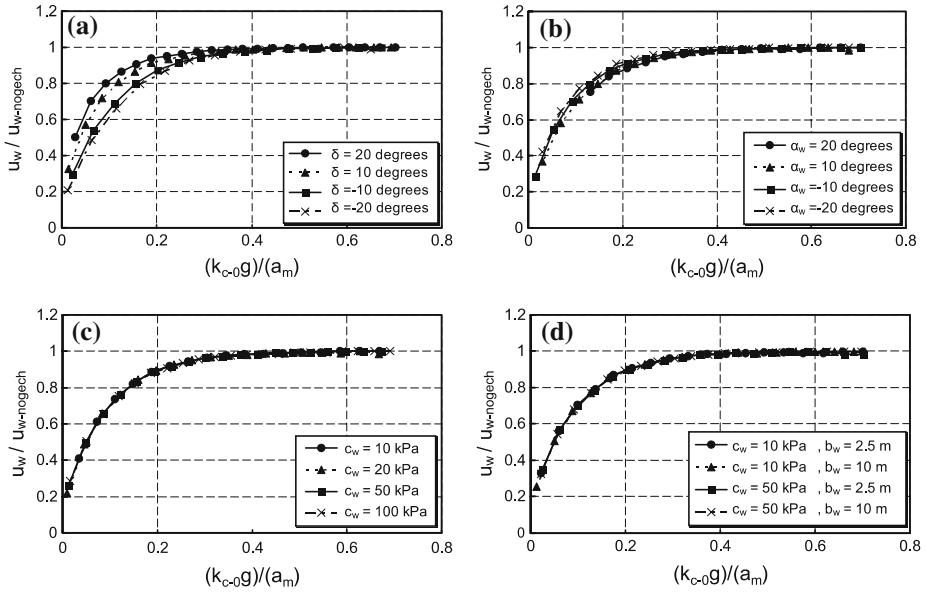

Fig. 7 The parametric analyses described in Tables 1 and 2. The ratio $u_w/u_{w-nogech}$, where $u_{w-nogech}$ is the seismic wall displacement when changes in the geometry of the soil behind the wall are neglected, versus the ratio $(k_{c-0}g)/a_m$ in terms of **a** the wall interface inclination, δ, **b** the inclination of the wall base, α_W, **c** the resistance of the wall base, c_w and **d** the length of the wall base, b_w

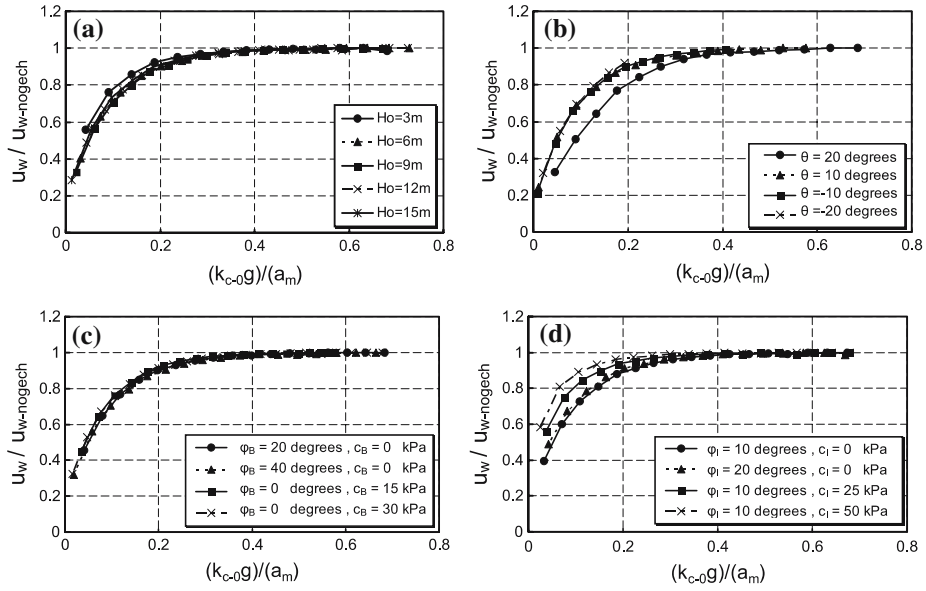

Fig. 8 The parametric analyses described in Tables 1 and 2. The ratio $u_w/u_{w-nogech}$, where $u_{w-nogech}$ is the seismic wall displacement when changes in the geometry of the soil behind the wall are neglected, versus the ratio $(k_{c-0}g)/a_m$ in terms of **a** the height of the backfill, H_0, **b** the inclination of the backfill, θ, **c** the resistance of the backfill, ϕ_B, c_B, and **d** the resistance of the wall-backfill interface ϕ_I, c_I

block model is over-conservative for the case of critical-to-applied-seismic acceleration ratios less than about 0.30, but works well for cases where this ratio ranges between 0.5 and 0.8.

Application procedure and limitations

The proposed model is intended for the prediction of the seismic displacement of gravity walls retaining dry soil of the general geometry given in Fig. 1. By "dry" soil it is meant that there is no water table and no pore water pressures. It is not implied that the water content is necessarily zero.

Similarly to the analysis of Kotta et al. (1988), it is recommended to accept performing one-dimensional equivalent-linear dynamic analyses to obtain the required acceleration time history. In these analyses, the soil profile including the soil retained by the wall should be considered. The input motion should be typical of the region and should be applied at the underlying bedrock. The effect of the shear strain on the shear modulus and the damping of soils should be considered. The acceleration time history required for the prediction of wall displacement should be obtained at a depth $2H_0/3$, where the height H_0 is defined in Fig. 1. This depth is the "representative" depth of the slip surface of the wall-backfill system.

The proposed model cannot be applied for backfill soils that exhibit considerable strain softening. In this case, the situation is more complex, as both the peak and the residual strengths play a role. Both the location of the slip line in the soil behind the wall at the initial configuration, and the change of the geometry with displacement may be affected by these two values of strength. The first phenomenon above is described by Iai (2001).

Evaluation of proposed methodology

Comparison with shaking-table test

The shaking-table test results by Nishimura et al. (1995) are first used to evaluate the proposed model. The configuration of the shaking-table tests is given in Fig. 9a. The geometrical and strength properties of the wall-backfill system tested were measured: $W_w = 3.54\,\text{kN/m}$, $H_0 = 0.36\,\text{m}$, $b_W = 0.45\,\text{m}$, $\alpha_W = \delta = \theta = 0°$, $\gamma = 16\,\text{kN/m}^3$, $\phi_B = 30°, \phi_w = 15°, \phi_I = 20°$ and $c_B = c_w = c_I = 0°$. The applied horizontal acceleration history at the base of the configuration is given in Fig. 10a. The measured wall displacement versus time is given in Fig. 10b. The observed final configuration of the wall-backfill system is given in Fig. 9a.

The proposed model predicts that $\alpha_{Bcr-0} = 49°$ and $k_{c-0} = 0.12$. As the horizontal acceleration was applied at the base of the backfill and the backfill has very small height, dynamic analysis was not performed. The acceleration history of Fig. 10a was applied to estimate the wall displacement. The computed accumulation of wall displacement with time with both the proposed model and Eq. 10 is given in Fig. 10c. When the proposed model was used, the computed final deformation of the wall-backfill system is given in Fig. 9b, the computed final wall displacement is 5.6 cm and the computed slip surface inclination at the final configuration is 47°. When Eq. 10,

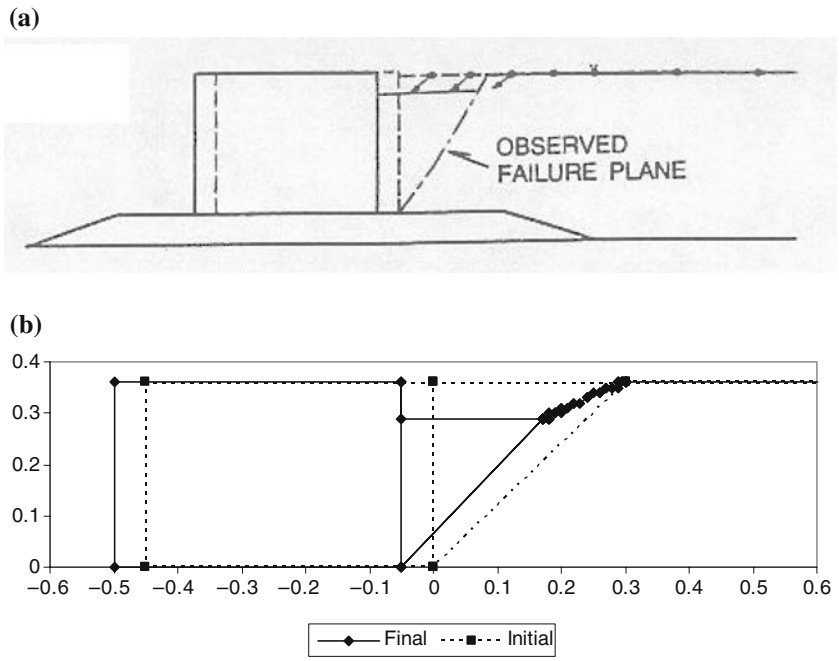

Fig. 9 The shaking-table tests by Mishimura et al. (1995). **a** Configuration of the tests and measured final deformation. **b** Predicted final deformation by the proposed model

which does not take into account changes in soil wedge geometry, was used, the final wall seismic displacement increased to 6.5 cm.

From Fig. 10, it can be observed that the computed displacement accumulation response agrees with the one measured. In addition, as shown in Fig. 9, the computed final deformation of the backfill agrees with the one measured. Furthermore, the ratio of computed by measured (a) wall displacement and (b) initial and final slip surface inclination is (a) 1.04 and (b) 0.98 and 0.94, respectively. When Eq. 10 was used, predictions are less accurate.

Prediction of response computed by elasto–plastic dynamic analysis

Full dynamic elasto–plastic analyses of a model concrete gravity wall 8 m high with W_w equal to 634 kN/m resting on a soil 30 m deep, shown in Fig. 11a, were recently performed (Modaressi and Lopez-Caballero 2001, Lopez-Caballero and Modaressi 2002). Both the retained and the foundation soil are normally consolidated clay above the water table. The retained soil has a plasticity index of 30% and uniform shear wave velocity, V_s, of 123 m/s. Below the wall, the plasticity index of the soil is 15% and V_s increases with depth: (a) From zero to 6 m below the base of the wall V_s equals 123 m/s, (b) from 6 to 12 m below the base of the wall V_s equals 200 m/s, (c) from 12 to 20 m below the base of the wall V_s equals 260 m/s and (d) from 20 to 30 m below the base of the wall V_s equals 325 m/s. The large-strain strength parameters of the soil and the wall-soil boundaries are $\phi_B = 26°, c_B = 0, \phi_W = 18°, c_w = 0$ and $\phi_I = 11°, c_I = 0$.

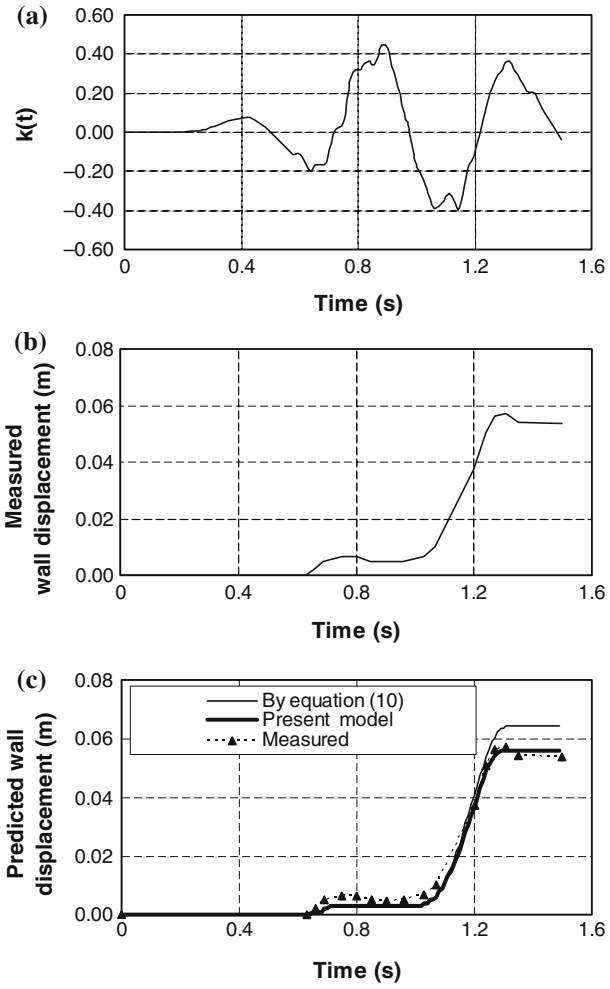

Fig. 10 The shaking-table tests by Mishimura et al. (1995). **a** Applied acceleration at the base and **b** measured and **c** predicted accumulation of wall displacement

The dynamic numerical analyses were performed using the GEFDYN Finite-Elements software. The Hujeux elastoplastic model was used to model the soil behaviour. The parameters of the Hujeaux model were such that when the shear strain increases, the stiffness degradation and the hysteretic damping computed are similar to those predicted by Vucevic and Dobry (1991) in terms of the plasticity index. Figure 12 compares computed stiffness degradation with that predicted by the Vucevic and Dobry (1991) curves.

As the lateral limits of the problem are considered to be far enough and only vertically propagating shear waves are studied, their response was assumed to be the response of a free field. Thus, equivalent boundaries have been imposed on the nodes of these boundaries (i.e. the normal stress on these boundaries remains constant and the displacements of nodes at the same depth in two opposite lateral boundaries are the same in all directions). The bedrock is supposed to be infinitely rigid with respect

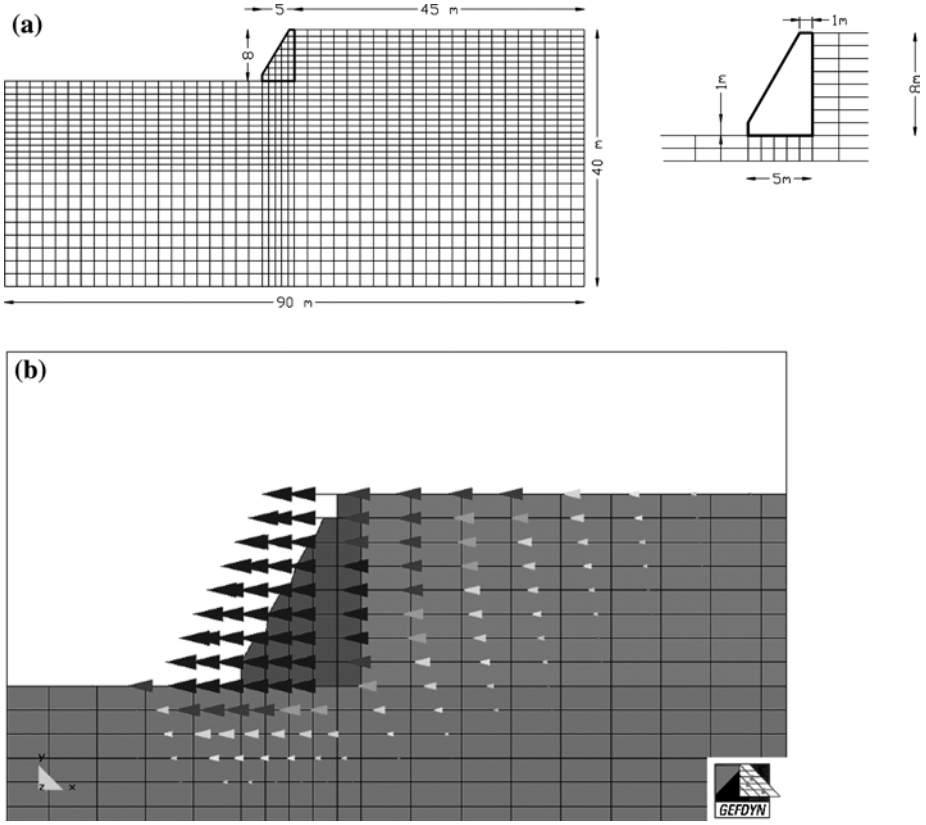

Fig. 11 The FEM elasto–plastic dynamic analyses by Modaressi and Lopez-Coballero. **a** The configuration considered and **b** the computed final horizontal deformation for the case of $a_{\mathrm{m-bedrock}} = 0.56$ g. The *vectors* (not scaled in favour of clarity) indicate the horizontal displacement of the nodes of the grid. The size and shading of the *arrows* also indicates the amplitude of horizontal displacements

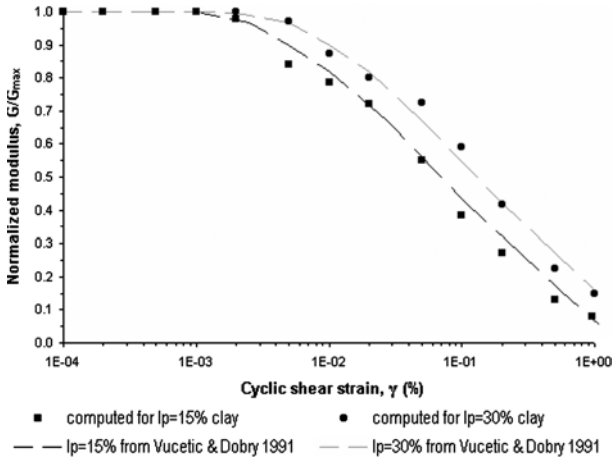

Fig. 12 The FEM elasto–plastic dynamic analyses by Modaressi and Lopez-Coballero. Comparison of the computed Shear Modulus reduction (*symbol lines*) and the Vucetic and Dobry (1991) *curves*

to the soil profile, and the computation has been done in a coordinate system following the input acceleration. Therefore, the nodes at the base of the mesh have been fixed and the acceleration history has been applied.

The Irpinia NS (Italy) Cairano 16/1/1981 acceleration history record, scaled to different values of maximum acceleration, was applied at the bedrock. This earthquake record has a fundamental period T_f of 0.3 s. The fundamental period of the soil stratum, including the backfill, corresponding to the small-strain moduli is 1.2 s. Table 3 gives the computed wall final horizontal displacement for the different values of maximum applied acceleration.

The parameters for the proposed simplified model of this problem are $W_w = 634\,\text{kN/m}$, $H_0 = 8\,\text{m}$, $b_W = 5\,\text{m}$, $\alpha_W = \delta = \theta = 0°, \gamma = 18\,\text{kN/m}^3$, $\phi_B = 26°$, $\phi_w = 18°, \phi_I = 11°$ and $c_B = c_w = c_I = 0°$. With these values, the model predicts $\alpha_{Bcr-0} = 54.2°$ and $k_{c-0} = 0.016$. One-dimentional equivalent linear elastic analyses were performed using the code Cyberquake (BRGM Software 1998) to obtain the representative acceleration history. According to the problem considered, a clay with plasticity and variation of shear velocity as described previously is assumed. The same (1) boundary conditions and applied accelerations at the base of the foundation soil and (2) equivalent shear modulus degradation and damping versus shear strain relations for the two types of clay (i.e. as predicted by the relationships of Vucetic and Dobry 1991) were used as in the elaborate elasto–plastic analyses.

Table 3 gives the wall displacement predicted by the proposed simplified method in terms of the maximum applied acceleration. Predictions are given for both (a) the bedrock record and (b) the acceleration history computed by the equivalent linear dynamic analyses at a depth of 5.3 m. Predictions using Eq. 10 are also given. Figure 12a gives the final deformation of the wall-backfill system as computed with the

Table 3 Wall displacement (u_W) computed by the elasto–plastic dynamic Finite Element Method (FEM) and predicted by the simplified proposed model when (a) the bedrock acceleration history is applied and (b) the acceleration history computed by the linear dynamic analyses at a depth of 5.3 m is applied

$a_{m-bedrock}$ (g)	u_{W-FEM} (cm)	u_W predicted by the simplified models (cm)				$(u_{W-predicted})/u_{W-FEM}$			
		The bedrock acceleration history is applied		The acceleration history computed by the linear dynamic analyses is applied		The bedrock acceleration history is applied		The acceleration history computed by the linear dynamic analyses is applied	
	(a)	I (b)	II (c)	I (d)	II (e)	(b)/(a)	(c)/(a)	(d)/(a)	(e)/(a)
0.11	15	2.0	2.5	15	27	0.13	0.17	1.00	1.77
0.28	33	10	14	36	73	0.30	0.33	1.09	2.22
0.33	38	13	19	41	86	0.34	0.39	1.08	2.27
0.39	45	16	25	48	101	0.36	0.44	1.07	2.25
0.56	63	26	44	69	147	0.41	0.56	1.10	2.33

Input motions of different magnitude are applied in the underlying rock. The estimated wall displacement by Eq. 10 is also given

I Predicted by the proposed model

II Predicted by Eq. 10

proposed simplified model for the case of $a_{\mathrm{m-bedrock}} = 0.56\,\mathrm{g}$ using the acceleration deduced by the linear dynamic analyses.

From Table 3 it can be observed that the values of seismic wall displacement predicted with the proposed simplified method compare well with the values computed by the dynamic elasto–plastic method. The wall displacement estimated by the proposed simplified model using the acceleration deduced by the linear dynamic analyses, divided by the wall displacement computed by the elasto–plastic dynamic method, for all five cases, varies between 1.00 and 1.10. In addition, from Table 3, it can be observed that the predictions by the proposed model are closer to the wall displacement computed in the elasto–plastic dynamic method than the predictions by Eq. 10, especially when the wall displacement is large. This is presumably because changes in the geometry of the retained soil as the wall moves outwards are not considered by Eq. 10.

For further qualitative validation, the deformation of the backfill computed by the elasto–plastic dynamic method is compared with the deformation mechanism estimated by the two-body simplified model. In particular, the horizontal displacement of the backfill is compared because in the elasto–plastic method earthquake-induced permanent deformation occurs as a result of both (1) shear strain and (2) volumetric strain, while the two-body simplified model simulates only the effect (1). Settlement is affected by both (1) and (2), while horizontal displacement is affected primarily by (1) only.

For the case of $a_{\mathrm{m-bedrock}} = 0.56\,\mathrm{g}$, Fig. 11b gives the final distribution of the horizontal displacement that is computed by the elasto–plastic dynamic method. In this figure, the vectors (not scaled in favour of clarity) indicate the horizontal displacement of the nodes of the grid. The size and shading of the arrows also indicates the amplitude of horizontal displacements. It can be observed that the horizontal deformation of the backfill decreases as (a) the horizontal distance from the wall increases and (b) the depth increases. The horizontal displacement is larger than (1) 70% and (2) 25% of its peak value inside soil wedges behind the wall with inclinations of about 45 and 30°, respectively.

On the other hand, as shown in Fig. 13, the two-body simplified method predicts that the horizontal deformation of the backfill decreases as (a) the horizontal distance

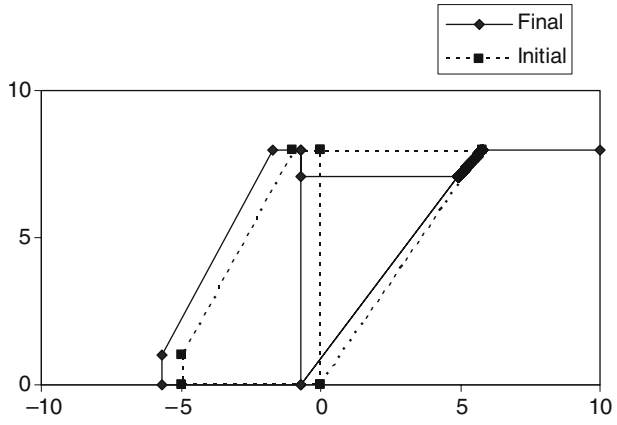

Fig. 13 The final deformation predicted by the proposed simplified method for the problem considered in the FEM elasto–plastic dynamic analyses by Modaressi and Lopez-Coballero for the case of $a_{\mathrm{m-bedrock}} = 0.56\,\mathrm{g}$

from the wall increases and (b) the depth increases. The horizontal displacement takes its peak value inside a soil wedge behind the wall with inclination of 54° and is zero outside a soil wedge behind the wall with inclination about of 50°. The gradual decrease of horizontal displacement with horizontal distance predicted by the two-body simplified model is a result of the incremental procedure used, where as the wall moves outwards, the cross-sectional area of the backfill that deforms changes.

It is inferred that the distribution of horizontal displacement of the two-body simplified model agrees qualitatively with that computed by the elasto–plastic dynamic method. Quantitavely, the deviation in the magnitude of the horizontal displacement at given horizontal distance from the wall can be interpreted by the fact that shear deformation at the elasto–plastic dynamic method develops as a result of both (1) shear strains without soil failure and (2) shear strains caused by momentary soil failure, while at the 2-block simplified method shear deformation develops as a result of only momentary soil failure.

Conclusions

Gravity walls retaining soil above the water table are modeled as a system of two bodies: (a) the gravity wall that slides along the wall-foundation soil boundary and (b) the critical wedge in the soil behind the wall. The strength of the system is defined by both the frictional and the cohesional components of resistance. The angle of the prism of the critical soil wedge behind the wall is obtained using the limit equilibrium method under earthquake loading. The model accounts for changes in the geometry of the backfill soil behind the wall considering displacements at each time step under limit equilibrium. Parametric analyses using the new method illustrated that the standard (single) block model is over-conservative for the extreme case of critical-to-applied-seismic acceleration ratios less than about 0.30, but works well for cases where this ratio ranges between 0.5 and 0.8. The method was applied successfully to predict the permanent wall displacement (a) measured in dynamic shaking-table tests and (b) computed by elasto–plastic dynamic analyses.

Acknowledgements This work was supported by (a) the European Commission, DG XII for Science, Research and Development (project ENV4-CT97-0392) and (b) the Hellenic Organization of Seismic Protection (OASP). Mr. Aris Stamatopoulos provided valuable comments. Mr. Stavros Aneroussis assisted in the case studies and parametric analyses.

References

Ambaseys N, Menu J (1988) Earhquake induced ground displacements. Earthq Eng Struct Dyn 16(7):985–1006

BRGM (French Geological Survey) Software (1998) Cyberquake, version 1.1, user's Guide. Cedex, France

Dahliquist G, Bjorck A, translated by Andeson N (1974) Numerical methods. Prentice-Hall Inc., NJ

Iai S (2001) Recent studies on seismic analysis and design of retaining structures. Fourth international conference on recent advances in geotechnical earthquake engineering and soil dynamics. San Diego, CA, March 26–31 (on CD)

Kotta N, Tsamis V, Gazetas G (1988) Seismic failure of Kalamata harbour Quaywall. Proceedings of the first hellenic conference on geotechnical engineering, vol II, pp 117–122 (in Greek)

Lopez-Caballero F, Modaressi A (2002) Importance of site effects in seismic induced displacements of gravity walls. 12th European Conference on Earthquake Engineering. Elsevier Science Ltd (on CD), Amsterdam

Modaressi A, Lopez-Caballero F (2001) Final report for the project "Seismic Ground Displacements as a tool for town planning, design and mitigation". Work performed by Ecole Centrale Paris, European Commission, DG12

Mononobe N (1924) Considerations on vertical earthquake motion and relevant vibration problems. J Jpn Soc Civil Eng 10(5):1063–1094 (in Japanese)

Newmark NM (1965) Effect of earthquakes on dams and embankments. Geotechnique 5(2):139–160

Nishimura Y, Fukui S, Sato M, Kurose H (1995) Shaking table tests and numerical simulation of seismic response of the seawall. Proceedings of third International Conference On Recent Advances in Geotechnical Earthquake Engineering and Soil Dynamics, Vol. 1, pp335–338

Okabe S (1924) General theory of earth pressure and seismic stability of retaining wall and dam. J Jpn Soc Civil Eng 10(6):1277–1323 (in Japanese)

Richards R, Elms D (1979) Seismic behaviour of gravity retaining walls. J Geotech Eng Division ASCE 105(4):449–464

Sarma SK (1999) Seismic slope stability — the critical acceleration. Proceedings of the second international conference on earthquake geotechnical engineering. Balkema, Lisbon, pp1077–1082

Stamatopoulos CA, Velgaki EG (2001a) Critical acceleration and seismic displacement of vertical gravity walls by a two body model. Fourth international conference on recent advances in geotechnical earthquake engineering and soil dynamics. San Diego, CA, March 26–31 (on CD)

Stamatopoulos CA, Velgaki EG (2001b) Seismic displacement of gravity walls with inclined surface retaining dry sand. Proceedings of second panhellenic conference in antiseismic engineering and technical seismology. Thessaloniki, November, volume A, pp117–125 (in Greek)

Stamatopoulos CA, Stamatopoulos AC, Aneroussis S, Velgaki EG (2001) Final Report for the project "Seismic Ground Displacements as a tool for town planning, design and mitigation". Work performed by Kotzias-Stamatopoulos Co., European Commission, DG12

Stamatopoulos C (1996) Sliding system predicting large permanent co-seismic movements of slopes. Earthq Eng Struct Dyn 25(10):1075–1093

Vucetic M, Dobry R (1991) Effect of soil plasticity on cyclic response. J Geotech Division ASCE 117(1):89–107

Whitman RV (1990) Seismic design and behavior of gravity retaining walls, Design and performance of earth retaining structures. Proceedings /GT Div. ASCE, Cornell University

Zarrabi - Kashani K (1979) Sliding of gravity retaining walls during earthquakes considering vertical accelerations and changing inclination of failure surface. S.M.Thesis, Department of Civil Engineering, MIT